Ab Initio and Variational Transition-State Theory Study of the $CF_3CF_2OCH_3$ + OH Reaction Using Integrated Methods: Mechanism and Kinetics

J. Espinosa-García*

Departamento de Química Física, Universidad de Extremadura, 06071 Badajoz, Spain

Received: July 22, 2002; In Final Form: December 13, 2002

The reaction of the OH radical with the fluorinated ether $CF_3CF_2OCH_3$ was studied by integrated ab initio electronic structure methods and variational transition-state theory with multidimensional tunneling. The OH radical attacks the three hydrogens of the methyl group, with two of these approaches being symmetric. In each hydrogen abstraction reaction, five stationary points (reactants, reactant complex, saddle point, product complex, and products) were located and characterized. A similarity was found between the three approaches of the OH radical, with energy differences of 0.1 kcal mol^{-1} for the barrier heights, and this allows one to assume that the dynamics for these hydrogen abstraction reactions will be very similar. Thus, the intrinsic reaction path was constructed for just one approach of the OH radical using the IMOMO integrated method, and the rate constant was calculated for the whole reaction as being thrice the rate constant for this approach for the temperature range 250−500 K using variational transition-state theory with multidimensional tunneling effect. The integrated method reproduced the behavior of the "model" reaction (CH_4 + OH) at the higher level, with substantial savings in computational cost. Variational effects and tunneling were found to be important, a behavior already known for the "model" system. The theoretical rate constants underestimated the experimental values, even though high ab initio electronic levels were used. This is a general problem in computational chemistry, associated with the one-particle and *n*-particle basis set limitations, and is not directly related to the integrated method used here.

1. Introduction

The kinetic and dynamic study of reactions involving large compounds (molecules and free radicals) represents an exciting challenge to the theoretical chemist because the application of high-level calculations is prohibitive. To circumvent this problem, i.e., large compounds/high-level calculations, two alternatives, mainly, can be used. One involves density functional theory (DFT).[1−5] It is well-known that DFT calculations or hybrid DFT calculations that mix in variable proportions of Hartree−Fock exchange yield reasonable geometries and vibrational frequencies,[6] atomization energies,[7] and enthalpies of formation.[8] However, when breaking−forming bonds are involved in the transition state zone, DFT and hybrid DFT fail to perform well[9−17] and generally underestimate the barrier height by several kcal mol^{-1}. However, several groups[18,19] have recently examined the influence of the proportion of Hartree−Fock exchange on the transition structure description, concluding that the fraction needed to predict accurate barrier heights differs from the optimal fraction needed to predict thermochemical properties and geometries, and new reparametrized DFT hybrid methods have been proposed to study particular reactions. In sum, the accuracy limitation of the DFT and hybrid DFT approaches dissuades one from using them for the reaction-path description.

An interesting and economical group of alternatives for the problem of large molecules and high-level calculations are the integrated methods, which describe different parts of the large system with different theoretical approaches. The main goal is to reproduce the results of a high-level theoretical calculation for a large, "complete" system, by dividing it into two parts: a small "model" system (which is the most active site, where the breaking−forming bonds are involved), and the "rest" of the molecular system. Different levels of theory are applied to these two parts: a higher-level for the model system and a lower-level for the complete system. Beginning with the pioneer work of Warshel and Levitt[20] in 1976, considerable effort has been made in this direction.[20−37] Thus, Morokuma and coworkers[25−31,37] have developed a number of useful strategies in this field. Recently, they developed the IMOMO method[28] (integrated ab initio molecular orbital−molecular orbital) where the model and the complete systems are described at two different MO levels. This method has been widely tested on several examples, including conformational analysis, geometry optimization, geometry, and energy analysis of the stationary points. They concluded[28] that the IMOMO method produces very similar results to the full higher level calculation for the complete system, and that the most important aspect of the method is its computational advantage.

The first studies were devoted to the analysis of stationary points with special attention to stable molecules. Comparatively, however, far less effort has been devoted to the study of the performance of the integrated methods in describing saddle points[28,38−43] and reaction paths.[39−47] Recently, our group has extended the idea of the integrated methods to the reaction-path construction in a chemical reaction and thence to studying the kinetics and dynamics. The new method was named RAIL (rate constant calculations with integrated levels)[43] and uses the IMOHC method of Corchado and Truhlar.[35,36] However, the use of IMOHC represents RAIL's main drawback, since the computational cost is increased by the "link" atom optimization. Later, we extended the study[44] using the IMOMO method. We

* Corresponding author. E-mail: joaquin@unex.es

10.1021/jp021700o CCC: $25.00
Published on Web 02/20/2003

concluded that the two integrated methods (IMOMO and IMOHC) behave similarly in predicting stationary point properties,[38] which reproduce the behavior of a benchmark calculation for kinetic and dynamic properties along the reaction path, and finally, that the success of these methods is mainly due to the higher-level model system description, showing little dependence on the low-level system, which was used in the computation.

In those first studies[43,44] we used small systems as test, CH_3-CH_3 + H in the first case[43] and CF_3CH_3 + OH in the second,[44] with the aim of checking the results against higher level ab initio calculations, which are otherwise not readily achievable, and in some cases prohibitive, for large systems. In the present paper we apply the integrated methodology to a larger system, CF_3-CF_2OCH_3 + OH. This reaction presents several important features that invite theoretical study. First, knowledge of the kinetics of partially fluorinated ethers with the hydroxyl radical, since these compounds are regarded as candidates to replace the Earth's ozone layer destroying CFCs (chlorofluorocarbons), is very important for understanding their role in atmospheric processes, especially in the chemistry of stratospheric ozone. Second, this reaction is a polyatomic reaction with 10 heavy atoms, which is hard to describe by ab initio calculations, especially the construction of the reaction path, where energy and first and second energy derivatives have to be calculated at a large number of points. Third, since it presents the heavy-light-heavy mass combination, it is a good candidate to present a large tunneling effect at low temperatures.[48,49]

2. Methods and Computational Details

2.1. Electronic Structure Calculations. Geometry, energy, and first and second energy derivatives of all stationary points were calculated using the IMOMO method[25−31,37] implemented in the GAUSSIAN 98 program.[50]

The "complete" system (CS) is the reaction

$$CF_3CF_2OCH_3 + OH \rightarrow [CF_3CF_2OCH_2\cdots H\cdots OH]^{\neq} \rightarrow CF_3CF_2OCH_2 + H_2O$$

which is calculated at a low MO level (LL) and is denoted (CS,-LL). The reaction of methane with the hydroxyl radical is the "model" system (MS)

$$CH_4 + OH \rightarrow [CH_3\cdots H\cdots OH]^{\neq} \rightarrow CH_3 + H_2O$$

which is calculated at a higher MO level (HL) and is denoted (MS,HL). The final integrated IMOMO method is then denoted (MS,HL): (CS,LL), and the energy of the complete system is approximated by

$$E_{CS}(I) = E_{CS}(LL) - E_{MS}(LL) + E_{MS}(HL) \qquad (1)$$

where (I) denotes integrated level. Stated in this way, eq 1 considers the integrated calculation as the inclusion of higher-level effects in a lower-level calculation for the complete system.[35]

In this paper, for the geometry optimization and frequency calculation, the MP2=FULL/6-31G(d,p) level (second-order Møller−Plesset perturbation theory with full electron correlation) was chosen as HL, while the HF/6-31G level (Hartree−Fock) was selected as LL. The choice of this low level is justified by the conclusions of earlier papers[33,38,43] that the integrated scheme shows little dependence on which low level is used. The integrated level is then

MP2=FULL/6-31G(d,p):HF/6-31G

where the colon-separated pair (X_1:X_2) denotes the integrated level used: X_1 is the higher-level for the model system and X_2 is the lower-level for the complete system. This level is denoted as Level 0.

At a second step, to improve the energy description of the stationary points, a single-point calculation is made at higher-levels, i.e., calculation of the energy at a higher integrated level using the geometry optimized in the previous step.

Level I. Using the geometries optimized at Level 0, a single-point calculation is made with a better description of the model system using the CCSD(T)[51] (coupled-cluster approach with single and double substitutions including a perturbative estimate of connected triple substitutions) with the 6-311++G(2df,p) basis set. This energy is denoted as

CCSD(T)/6-311++G(2df,p):
HF/6-31G//MP2=FULL/6-31G(d,p):HF/6-31G

where the double slash (X//Y) denotes geometry optimization at level Y and energy calculated at level X, both integrated levels.

Level II. Continuing with the CCSD(T) approach, an enlarged basis set is used, namely, the correlation-consistent polarized valence triple-ζ developed by Dunning and co-workers (cc-pVTZ).[52] This integrated energy is denoted as

CCSD(T)/cc-pVTZ:HF/6-31G//MP2=FULL/6-31G(d,p):
HF/6-31G

2.2. Dynamics Calculations. At the MP2=FULL/6-31G(d,p):HF/6-31G integrated Level 0, the "intrinsic reaction coordinate" (IRC), or minimum energy path (MEP), is constructed starting from the saddle point geometry and going downhill to both the asymptotic reactant and product channels in mass-weighted Cartesian coordinates with a gradient step size of 0.02 bohr $amu^{1/2}$. The Hessian matrix was evaluated at every point along the reaction-path, always avoiding the undesirable reorientations of molecular geometries. Along this MEP the reaction coordinate, s, is defined as the signed distance from the saddle point, with $s > 0$ referring to the product side. In the rest of the work the units of s are bohr, and the reduced mass to scale the coordinates[53] is set to 1 amu. This has no effect on calculated observables, but it does affect the magnitude of s in plots used for interpretative purposes.

Along the MEP, a generalized normal-mode analysis was performed projecting out frequencies at each point along the path.[54] With this information, the ground-state vibrationally adiabatic potential curve was calculated:

$$V_a^G(s) = V_{MEP}(s) + \epsilon_{int}^G(s) \qquad (2)$$

where $V_{MEP}(s)$ is the classical energy along the MEP with its zero energy at the reactants ($s = -\infty$), and $\epsilon_{int}^G(s)$ is the zero-point energy at s from the generalized normal-mode vibrations orthogonal to the reaction coordinate.

Finally, the energies, vibrational frequencies, geometries, and gradients along the MEP were used to estimate the rate constants by using variational transition state theory (VTST). Thermal rates were calculated using the canonical variational theory[48,55] (CVT) approach which locates the dividing surface between reactants and products at a point $s_*^{CVT}(T)$ along the reaction path that minimizes the generalized TST rate constants, k^{GT}-(T,s) for a given temperature T. Thermodynamically, this is equivalent to locating the transition state at the maximum $\Delta G^{GT,o}$ $[T,s_*^{CVT}(T)]$ of the free energy of activation profile $\Delta G(T,s)$.[48,55]

Thus, the thermal rate constant will be given by

$$k^{\mathrm{CVT}}(T) = \sigma \frac{k_{\mathrm{B}}T}{h} K^{\mathrm{o}} \exp[-\Delta G(T,s^{*,\mathrm{CVT}})/k_{\mathrm{B}}T] \qquad (3)$$

with k_B being Boltzmann's constant, h Planck's constant, σ the symmetry factor (the number of equivalent reaction paths), and K^o the reciprocal of the standard-state concentration, taken as 1 molecule cm^{-3}.

The present work used the general polyatomic rate constants code GAUSSRATE,[56] which is an implementation based on the GAUSSIAN 98[50] and the POLYRATE[57] programs. Note that the current version of GAUSSRATE is based on the GAUSSIAN 94 program, which does not implement the IMOMO method. In the present work, therefore, some subroutines were modified in order to run the GAUSSIAN 98 program, which does include the IMOMO method. Since integrated methods are used, this version of GAUSSRATE is equivalent to our RAIL method. The rotational partition functions were calculated classically and the vibrational modes were treated as quantum-mechanical separable harmonic oscillators, with the generalized normal modes defined in redundant curvilinear coordinates.[58,59] The curvilinear coordinates chosen were all the possible bond lengths and angles. The advantage of curvilinear coordinates (nonlinear functions of Cartesian coordinates) over rectilinear ones (linear functions of Cartesian coordinates) is that in some cases the lowest bending frequencies have unphysical imaginary values over a wide range of the reaction coordinate using rectilinear coordinates, whereas these frequencies are real over the whole of the reaction-path using curvilinear coordinates. This behavior has been observed in other hydrogen abstraction reactions,[60−62] although for this large system, with 42 degrees of freedom, it was only possible to reduce the number of imaginary values. Thus, on the reactant side all frequencies are real, but on the product side the two lowest frequencies are still imaginary. Therefore, these two lowest frequencies were adjusted to real values by interpolating information from the reactants, products and saddle point. The calculation of electronic partition functions included the two electronic states for the OH reactant, with 140 cm^{-1} splitting. For the tunneling contribution, as information is only available on the reaction-path, centrifugal-dominant small-curvature tunneling (SCT)[63] was used. Methods for large curvature cases have been developed,[64] but they require more information about the PES than was determined in the present study.

3. Results and Discussion

3.1. Mechanism of Reaction. The optimized geometries of reactant ($CF_3CF_2OCH_3$) and product ($CF_3CF_2OCH_2$), using the IMOMO Level 0 method, are shown in Figure 1, and the corresponding harmonic vibrational frequencies are listed in Table 1. The largest geometric changes are on the $-CH_3$ center, where the bonds are broken, the rest of the molecular system, CF_3CF_2O-, being practically unaltered. Unfortunately, to the best of our knowledge, there are no experimental values for comparison.

When the hydroxyl radical attacks the methyl group of the reactant, three approaches (on each of the three hydrogens) are possible, two of those equivalent (on the hydrogens denoted H_2 and H_3 in Figure 1). Therefore, just two approaches were considered: one, abstraction of the H_1 hydrogen located in the plane defined by the three carbons (approach 1), and the other, abstraction of the H_2 hydrogen located out of that plane (approach 2). We shall begin by analyzing the hydrogen

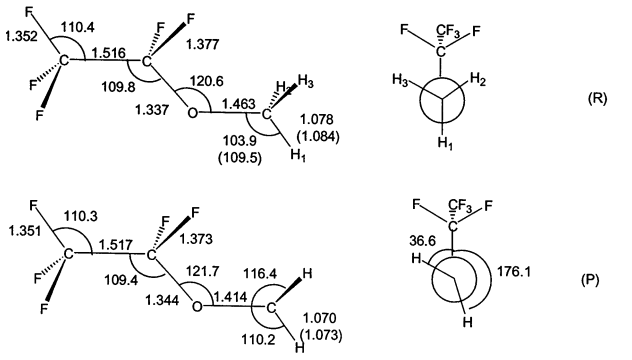

Figure 1. Optimized reactant and product geometries at Level 0 for the complete system. In parentheses the values at the MP2=FULL/6-31G(d,p) level for the model system, $CH_4 + OH$.

TABLE 1: Harmonic Vibrational Frequencies (cm^{-1}) and Zero-Point Energy (ZPE, in kcal mol^{-1}) for Reactant and Product at the Integrated Level 0

$CF_3CF_2OCH_3$	$CF_3CF_2OCH_2$	$CF_3CF_2OCH_3$	$CF_3CF_2OCH_2$
3354 (3283)[a]	3493 (3440)[b]	828	642
3347 (3283)	3323 (3440)	746	620
3217 (3283)	(3243)	643	542
(3135)		619	533
1581 (1627)	1574 (1491)	543	403
1569 (1627)	1530 (1491)	533	401
1566 (1406)	1395	402	370 (395)
1533 (1406)	1384	397	300
1384 (1406)	1381	368	233
1381	1290	298	182
1374	1240	235	
1274	1220	172	170
1253	1102	145	
1215	829	78	81
1207	750	68	68
1030	725		
ZPE 46.26	ZPE 36.8		

[a] Values for CH_4 at the higher level [MP2=FULL/6-31G(d,p)] are given in parentheses. [b] Values for CH_3 at the higher level [MP2=FULL/6-31G(d,p)] are given in parentheses.

abstraction reaction on the H_1 hydrogen (approach 1). On the $CF_3CF_2OH_2C\cdots H_1\cdots OH$ reaction path, the reaction of the OH radical with the molecule proceeds via a weakly reactant hydrogen bonded complex (denoted CR1), a saddle point (denoted SP1), and a product hydrogen bonded complex (denoted CP), as shown in Figure 2. The first stationary point (CR1) is a complex stabilized by two hydrogen-bonds, with a bond distance $O\cdots H_1$ of 2.509 Å. The other bond lengths and bond angles are very close to those of the separated reactants. Subsequently, shortening of the $O\cdots H_1$ interatomic distance led us to a second stationary point, which is a saddle point (SP1). The length of the bond that is broken ($C-H_1$) increases by 15% and the length of the bond that is formed (H_1-O) increases by 25%, with respect to $CF_3CF_2OCH_3$ and H_2O, respectively. Therefore, the reaction of the OH radical with the molecule proceeds via an "early" transition state, which is the expected behavior that would follow from Hammond's postulate,[65] since the reaction is exothermic (see Table 4). Finally, a third stationary point was found on the product side, which is also a complex stabilized by three hydrogen bonds (CP).

The three stationary points (CR1, SP1 and CP) were all identified by means of the eigenvalues of the Hessian matrix: the complexes are minima on the potential energy surface with all frequencies real, and the saddle point has one and only one negative eigenvalue and, therefore, one imaginary frequency. The corresponding eigenvector is associated with the broken

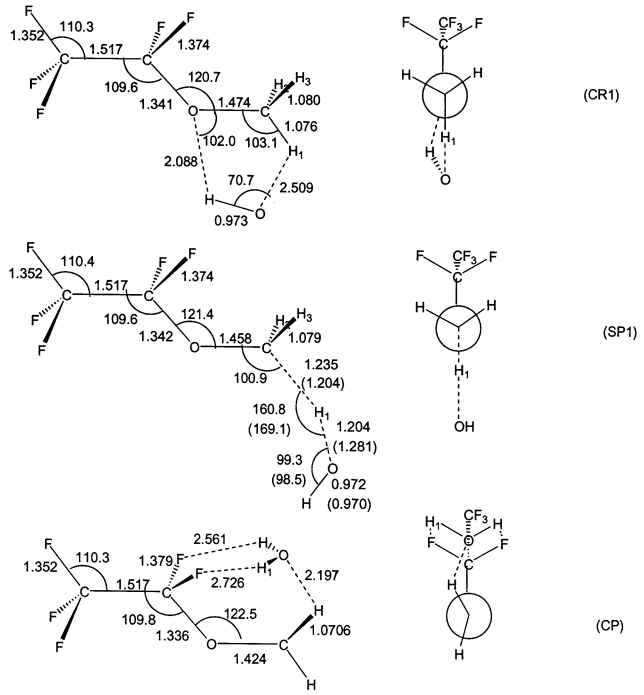

Figure 2. Optimized stationary point geometries at Level 0 for approach 1. CR1 reactive complex, SP1, saddle point, CP, product complex. In parentheses the values at the MP2=FULL/6-31G(d,p) level for the model system, CH_4 + OH.

TABLE 2: Harmonic Vibrational Frequencies (cm^{-1}) and Zero-Point Energy (ZPE, in kcal mol^{-1}) for Approach 1 at the Integrated Level 0

CR1	SP1	CP	CR1	SP1	CP
3822	3830 (3845)[a]	4023	644	679	614
3377	3369 (3322)	3891	621	642	541
3339	3244 (3318)	3495	545	612	534
	(3177)		536	543	403
3214	1613 (1545)	3308	459	532	403
1598	1572 (1521)	1692	407	402	376
1575	1533 (1465)	1578	393	392	347
1565	1390 (1327)	1536	368	366 (356)	309
1528	1381	1402	348	317 (292)	302
1386	1378	1383	301	278	238
1380	1290	1383	232	251	207
1371	1271	1260	194	230	202
1289	1253	1250	168	168	134
1254	1212 (1207)	1212	140	105	122
1224	1125	1083	112	76	119
1210	1035 (940)	826	72	73	82
1005	896	745	63	22 (31)	75
832	836	641	3	1868i (2060i)	40
747	763 (744)	621			
ZPE 53.36	ZPE 49.58	ZPE 52.00			

[a] Values for CH_4 + OH saddle point at the higher-level [MP2=FULL/6-31G(d,p)] are given in parentheses.

and formed bonds (Table 2). The small geometrical variations between the complexes and reactant or product cause very few changes in the harmonic vibrational frequencies of the complexes. The lowest values of the complexes correspond to restricted motions that previously were free rotations and translations of the reactants or products, and these vibrational modes would be expected to have very low frequencies.

Next, we shall analyze the second approach of the OH radical, i.e., the hydrogen abstraction reaction of the H_2 hydrogen (approach 2). In this case, the reaction evolves in a similar way as approach 1, and is shown in Figure 3. First, a weak reactant hydrogen-bonded complex (denoted CR2) is found, stabilized

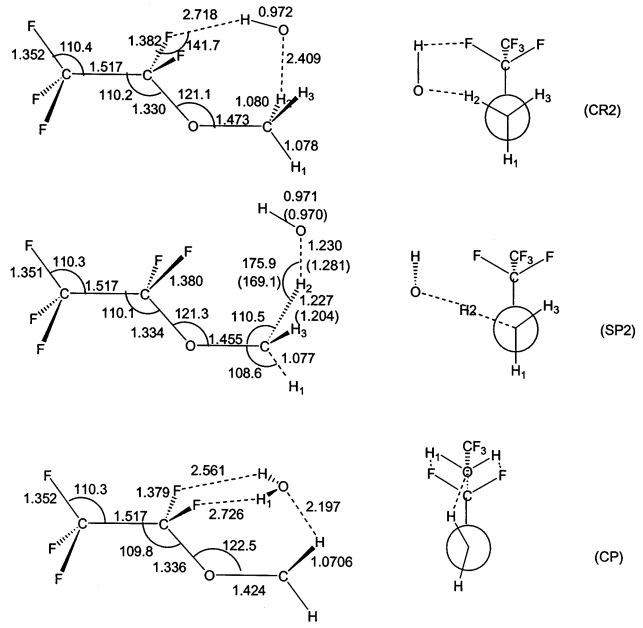

Figure 3. Optimized stationary point geometries at Level 0 for approach 2. CR2 reactive complex, SP2, saddle point, CP, product complex. In parentheses the values at the MP2=FULL/6-31G(d,p) level for the model system, CH_4 + OH.

TABLE 3: Harmonic Vibrational Frequencies (cm^{-1}) and Zero-Point Energy (ZPE, in kcal mol^{-1}) for Approach 2 at the Integrated Level 0

CR2	SP2	CP	CR2	SP2	CP
3853	3845 (3845)[a]	4023	642	676	614
3364	3386 (3322)	3891	618	641	541
3350	3267 (3318)	3495	542	616	534
	(3177)		532	542	403
3218	1580 (1545)	3308	403	533	403
1588	1546 (1521)	1692	396	405	376
1576	1527 (1465)	1578	370	398	347
1574	1392 (1327)	1536	340	371 (356)	309
1538	1384	1402	302	327 (292)	302
1386	1381	1383	241	285	238
1382	1315	1383	228	244	207
1377	1257	1260	198	218	202
1251	1241	1250	155	168	134
1247	1203 (1207)	1212	120	132	122
1231	1148	1083	88	109	119
1196	1042 (940)	826	81	70	82
1008	866	745	62	15 (31)	75
824	824	641	17	2146i (2060i)	40
745	740 (744)	621			
ZPE 52.96	ZPE 49.60	ZPE52.00			

[a] Values for CH_4 + OH saddle point at the higher-level [MP2=FULL/6-31G(d,p)] are given in parentheses.

by two hydrogen-bonds, with a bond distance O···H_2 of 2.409 Å, the other geometric parameters being very close to those of the separated reactants. Second, there is a saddle point (SP2) with increases of the lengths of the bonds broken/formed that are practically the same as in SP1, 14% and 28%, respectively, i.e., an "early" transition state. Finally, there is a third stationary point in the product valley, which is the same as that found in approach 1, i.e., the CP complex stabilized by three hydrogen-bonds.

The vibrational analysis confirmed the nature of these stationary points (Table 3). Thus, CR2 is a minimum on the potential energy surface, and SP2 has one and only one imaginary frequency associated to the broken/formed bonds. The absolute value (2146 i cm^{-1}) is slightly larger than the corresponding value for SP1 (1868 i cm^{-1}).

TABLE 4: Energy and Enthalpy (0 and 298 K) Changes Relative to Reactants (kcal mol^{-1}) at Several Integrated Levels

	Approach 1		Approach 2			
level	CR1	SP1	CR2	SP2	CP	P
ΔE						
level 0	−5.60	10.70	−4.73	11.01	−17.36	−10.40
lLevel I	−4.25	7.28	−2.83	7.26	−17.18	−10.93
level II	−4.50	6.81	−2.97	6.91	−17.90	−11.00
model reaction		12.06				−9.88
ΔH (0 K)						
level 0	−4.00	8.52	−3.53	8.83	−17.12	−11.57
level I	−2.65	5.10	−1.63	5.10	−16.94	−12.10
level II	−2.90	4.63	−1.77	4.75	−17.67	−12.17
model reaction		10.34				−11.58
ΔH (298 K)						
level 0	−3.69	8.33	−3.02	8.60	−16.33	−11.28
level I	−2.34	4.91	−1.12	4.87	−16.15	−11.81
level II	−2.59	4.44	−1.26	4.52	−16.88	−11.88
model reaction		10.00				−11.10

[a] Model reaction: $CH_4 + OH$ at the MP2=FULL/6-31G(d,p) single level.

3.2. Relative Energies. The changes in energy (ΔE) and enthalpy (ΔH, 0 and 298 K) of all the stationary points relative to the reactants are listed in Table 4 for several integrated levels. Note that ΔH (0 K) is ΔE corrected with the zero-point energy, and ΔH (298 K) includes the thermal corrections at 298 K.

We shall begin by analyzing the energy of reaction. The theoretical values have little dependence on the level of calculation (last column in Table 4), and unfortunately direct comparison with experiment is not possible because neither the enthalpy of reaction nor the enthalpies of formation of the molecule and radical have been measured experimentally. However, an estimate of the accuracy of the results can be obtained by considering the behavior of the $CF_3CH_3 + OH$ reaction studied previously,[44] where the enthalpy of reaction is known experimentally. In that work, at Level II the enthalpy of reaction (0 K) was found to be slightly underestimated (1.4 kcal mol^{-1}) with respect to experiment. Therefore, assuming a similar error for the present reaction at the same Level II, the enthalpies of reaction would be −13.57 (0 K) and −13.28 (298 K) kcal mol^{-1}.

Let us now consider the hydrogen-bonded complexes. The reactive complexes (CR1 and CR2) appear at an energy lower than that of the reactants, −5.60 and −4.73 kcal mol^{-1}, respectively. These stabilities diminish (i) when the level of calculation rises, −4.50 and −2.97 kcal mol^{-1}, respectively, at Level II, (ii) when the zero-point energy (0 K) is included, −2.90 and −1.77 kcal mol^{-1}, respectively, and (iii) when the thermal corrections (298 K) are included, −2.59 and −1.26 kcal mol^{-1}, respectively. The product complex (CP), stabilized by three hydrogen bonds, is 6.90 kcal mol^{-1} more stable than the products at Level II, and this difference has little dependence on the level of calculation. When the ZPE (0 K) and thermal corrections (298 K) are included, this stability of the complex diminishes, −5.50 and −5.00 kcal mol^{-1}, respectively.

With respect to the barrier heights, direct comparison with experiment is not possible for either approach (1 or 2). Raising the calculation level (Level 0 → Level II) lowers the barrier height by several kcal mol^{-1}, and it may be expected that a more accurate barrier height would be obtained using highly correlated wave functions and larger basis sets, which is beyond our computational capacity. To obtain an estimate of the limitations, the model reaction $CH_4 + OH$, which has been extensively studied at very high levels, was analyzed. Table 5 lists the most recent results.[17,66−69] When highly correlated wave functions and large basis sets are used (in some cases in combination with extrapolated approaches), the barrier height ranges from 4.97 to 5.83 kcal mol^{-1}, i.e., ≈ 1−2 kcal mol^{-1} lower than the CCSD(T)/cc-pVTZ result, which is equivalent to the highest level used here, Level II. The exceptions are Lynch and Truhlar's result,[17] which yields a value of 7.45 kcal mol^{-1} (see Table 5), and Lynch and Truhlar's estimate[17,70] of the true barrier height, based on analyzing experiments, which is slightly higher, 6.7 kcal mol^{-1}. Interestingly, the error in the barrier height is equivalent to our error estimate of the reaction energy. Therefore, these comparisons indicate that the barrier height for the complete system using integrated methods will be overestimated by at least this same amount. Masgrau and co-workers[69] pessimistically reported that, even though they used the highest ab initio electronic level reported up to now for dynamics calculations of the $CH_4 + OH$ reaction, the experimental rate constants were not reproduced exactly. Clearly, this situation will become worse in the case of larger systems, such as the title reaction.

TABLE 5: Barrier Height (kcal mol^{-1}) for the $CH_4 + OH \rightarrow CH_3 + H_2O$ Model Reaction at Several Very High Ab Initio Levels

method	$\Delta E^{\ddagger}$	$\Delta H^{\ddagger}$ (0K)	5ef
CBS/QCI/APNO	5.11		66
G2		5.9	67
G2M	5.3		68
MP2/cc-pVTZ	8.38	7.01	69
MP2/aug-cc-pVTZ	7.96	6.48	69
CCSD(T)/6-311++G(2df,2p)	7.45		17
CCSD(T)/cc-pVTZ	7.08	5.71	69
CCSD(T)/aug-cc-pVTZ	5.83	4.46	67
CCSD(T)-SAC/cc-pVTZ	4.97	3.60	69

The two saddle points (SP1 and SP2) present very small differences (0.3 kcal mol^{-1}) at the simplest IMOMO Level 0, and interestingly they show a similar tendency with the level of calculation. The similarity between the geometries, frequencies and energies of the two saddle points allows one to assume that the dynamics for the two surfaces will be very similar and that the three surfaces (remember that SP2 is obtained in an attack on the H_2 hydrogen, but that the attack on the symmetric H_3 hydrogen is equivalent) make almost equal contributions to the rate. Clearly, this assumption represents a substantial savings in computational cost considering the molecular size.

3.3. The "Model" Reaction. To help understand the influence of the description of the model reaction, $CH_4 + OH \rightarrow CH_3 + H_2O$, on the geometry, vibrational frequency, and energies of the IMOMO method, Figures 1−3 and Tables 1−3 also present these magnitudes for the model reaction at the high-level MP2=FULL/6-31G(d,p). First, the geometries of the reactant and the product agree with the model part (inner layer) of the IMOMO method, with the exception of the pyramidalization of the CH_3 radical, which is known to be planar. The broken and formed bonds and the angle of the saddle point in the model reaction reproduce the behavior of the complete system for both approaches 1 and 2. Thus, the bond that is broken ($C-H_1$) increases by only 11%, and the length of the bond that is formed (H_1-O) increases by 33%. This transition state is also "early", which is consistent with the exothermicity of the model reaction (Table 4).

Second, the common frequencies in the model reaction (values in parentheses in Tables 1−3) and the complete system are in reasonable agreement. The imaginary frequency, 2060 i cm^{-1}, at the saddle point is close to the values in the complete systems (SP1 and SP2).

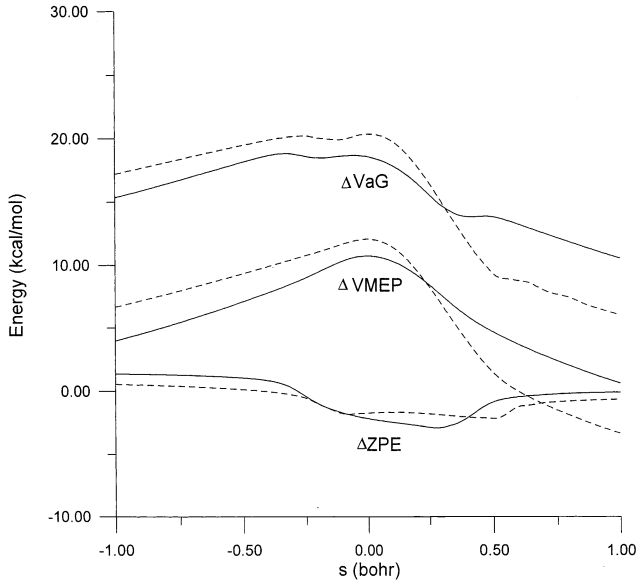

Figure 4. Classical potential energy (V_{MEP}), vibrationally adiabatic potential energy (ΔV_a^G) and zero-point energy (ΔZPE) curves with respect to the reactants as a function of *s*, for complete/IMOMO (solid line), and model/MP2 (dashed line).

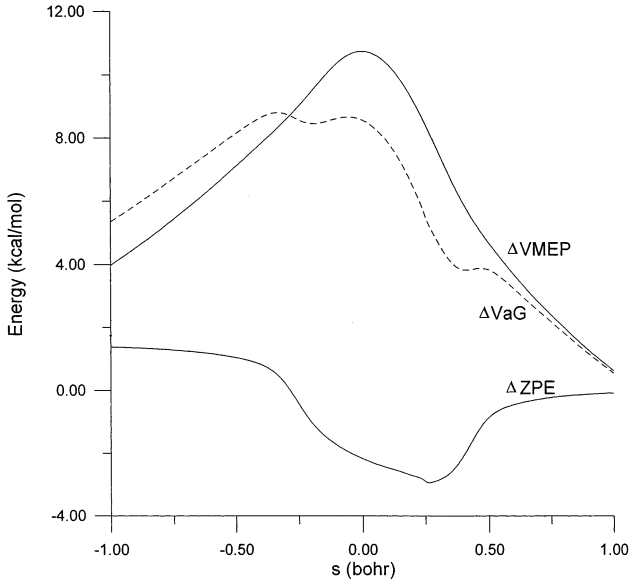

Figure 5. Classical potential energy (V_{MEP}), vibrationally adiabatic potential energy (ΔV_a^G), and zero-point energy (ΔZPE) curves with respect to the reactants as a function of *s* for the complete system at the IMOMO level, using curvilinear coordinates.

Third, the model reaction simulates the energy and enthalpy (0 K) changes (reaction and activation) of the complete system at similar levels, MP2 for the model reaction and Level 0 for the complete system.

Therefore, in the light of this comparison, it seems that the success of the IMOMO method is mainly due to the HL model system description, and the effects of the remaining LL fragments are smaller. This conclusion agrees with earlier studies by our group[38,43,44] using integrated methods.

3.4. Reaction-Path Analysis. Having analyzed the stationary points of the two approaches, and assuming similarity between them, we shall now extend the IMOMO scheme to construct the reaction path for approach 1. As mentioned above, the rate constant for the whole reaction is calculated as thrice the rate constant for one of the surfaces, in particular that of approach 1, which presents the lowest barrier height. The analysis of the reaction-path for approach 1 was carried out on the information (energy, gradient, and Hessian) at the integrated Level 0 [MP2=FULL/6-31G(d,p):HF/6-31G] over the *s* range −1.3 to +2.0 bohr. Further down the reactant valley, there were problems of convergence. For comparison purposes, the reaction path was also constructed for the model reaction, CH_4 + OH, at the single higher level, MP2=FULL/6-31G(d,p), in this case, over the *s* range −1.0 to +1.0 bohr.

We shall begin by comparing these two cases in the common *s* range (−1.0 to +1.0 bohr) using rectilinear coordinates. The classical energy along the MEP, V_{MEP}, the ground-state vibrationally adiabatic potential energy, ΔV_a^G, and the change in the local zero-point energy, ΔZPE, curves as a function of *s* over the common range are shown in Figure 4. Note that ΔV_a^G and ΔZPE are defined as the difference between these magnitudes at *s* and their values for the reactants. Again, the model reaction reproduces the energy, V_{MEP}, enthalpy at 0 K, ΔV_a^G, and zero-point energy change, ΔZPE, of the complete system at the same level, indicating that the success of the integrated method is mainly due to the high-level model system description.

We now analyze the complete system at Level 0. Figure 5 shows the V_{MEP}, the ΔV_a^G, and the ΔZPE, as a function of *s*, and Figure 6 shows some vibrational frequencies along the MEP. The behavior is that expected in hydrogen abstraction reactions,

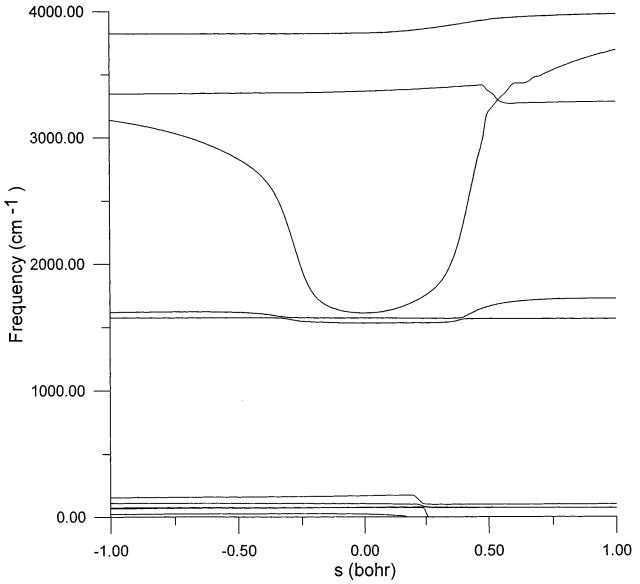

Figure 6. Some generalized normal-mode vibrational frequencies plotted versus *s*.

thus indicating the success of the integrated method in the description of this type of reaction. The mode related to the breaking (C−H_1)/forming(H_1−O) bonds drops dramatically near the saddle point (reactive mode). This mode presents a widening of the vibrational well, an effect which has been found in other reactions with a small skew angle.[44,49,71,72] The lowest vibrational frequencies along the reaction-path (transitional modes) correspond to the transformation of free rotations or free translations of the reactant limit into vibrational motions in the overall system. They present very small values along the reaction path, reaching their maximum in the saddle point zone. Therefore, in the saddle point region, the behavior of these transitional modes only partially compensates the fall in the ZPE caused by the reactive mode, and as a result the ZPE shows noticeable changes with *s* (Figure 5).

3.5. Improved Reaction Path. The poor energy description with the integrated Level 0 (see section 3.2 and Table 4) means that the integrated reaction path has to be optimized. In previous

TABLE 6: Rate Constants for the $CF_3CF_2OCH_3$ + OH Reaction[a]

	scaled[b]				fitted[c]	
T(K)	TST	CVT	SCT	CVT/SCT	CVT/SCT	exp.[d]
250	8.01(−18)[e]	7.44(−18)	10.05	7.48(−17)	3.24(−15)	4.52(−15)
275	2.39(−17)	2.20(−17)	6.56	1.44(−16)	4.77(−15)	7.83(−15)
300	6.00(−17)	5.52(−17)	4.82	2.66(−16)	6.84(−15)	1.24(−14)
350	2.65(−16)	2.39(−16)	3.18	7.60(−16)	1.29(−14)	2.54(−14)
400	8.43(−16)	7.40(−16)	2.44	1.80(−15)	2.23(−14)	2.54(−14)
430	1.51(−15)	1.30(−15)	2.17	2.82(−15)	2.98(−14)	5.67(−14)
500	4.65(−15)	3.86(−15)	1.79	6.91(−15)	5.40(−14)	

[a] The overall rate constants are obtained by multiplying the values for approach 1 by 3, in accordance with the three possibilities of the hydrogen abstraction reaction and the mechanism studied in this paper. [b] The scaled values correspond to Level 0 × 0.636, $\Delta E^{\neq} = 6.81$ kcal mol^{-1}. [c] The fitted values correspond to Level 0 × 0.350, $\Delta E^{\neq} = 3.75$ kcal mol^{-1}. [d] Reference 77. $K(CF_3CF_2OCH_3) = (1.90_{-0.61}{}^{+0.90} \times 10^{-12} \exp[-(1510 \pm 120)/T]$, cm^3 molecule^{-1} s^{-1}, over the temperature range 250−430 K. [e] 8.01(−18) stands for 8.01×10^{-18}, in cm^3 molecule^{-1} s^{-1}.

papers[71,73,74] we analyzed different approximations and found that the best choice was to scale the original curve (MP2:HF Level 0) regularly by a factor

$$F = \Delta E(\text{MP2:HF}, s{=}0)/\Delta E(\text{Level II}, s{=}0)$$

where ΔE is the variation of energy at each level with respect to the reactants. At the saddle point, $s = 0$, the barrier height is that of the highest level, Level II in this case. This factor is 0.636.

3.6. Rate Constants. The bottleneck properties of the reaction, based on the CVT approach, show that the location of the generalized transition state (GTS) is away from the saddle point: from −0.363 to −0.356 bohr over the temperature range 250−500 K. Thus the variational effects, i.e., the ratio between the variational CVT and conventional TST rate constants, are important. This result agrees with the behavior of the model system, CH_4 + OH,[69,75,76] and with the behavior found in our earlier work with the CF_3CH_3 + OH reaction,[44] which also present large variational effects.

In Table 6 the calculated conventional TST and variational CVT rate constants at the scaled Level 0 (factor 0.636, Level II reference, $\Delta E^{\neq} = 6.81$ kcal mol^{-1}) are compared to experimental values[77] in the temperature range 250−500 K. First, the difference between the TST and CVT rates confirms the above conclusion about the variational effects. Second, the tunneling effect is important in this temperature range, and comparable to the results obtained with the model reaction, CH_4 + OH,[76] indicating again the importance of an appropriate description of the model reaction. Finally, the theoretical results strongly underestimate the experimental data, by factors of 60 to 20 in the common temperature range 250−430 K. The problem arises from the use of an incomplete basis set, and from the partial introduction of correlation energy at the CCSD-(T) level. It should be noted that this limitation is not due to the nature of the integrated method, since this same problem is found for the model system using high ab initio electronic structure calculations.[69]

To match the experimental data, two effects must be considered: the tunneling effect of large curvature (LC) and the barrier height. As we have already indicated, the LC method requires more information about the PES than that was determined in this study. However, we can estimate this effect considering the "model reaction" CH_4 + OH.[76] We obtained a factor LC/SCT ranging from 1.5 to 1.1 over the temperature range 250−500 K. We can assume this behavior for the title reaction. With respect to the second factor, one has to continue lowering the barrier height. Taking into account the influence of the LC tunneling effect (which has not been directly calculated in this paper), reasonable agreement was found when the barrier height was 3.75 kcal mol^{-1} (fitted-Level 0 values in Table 6). Interestingly, this value is close to the barrier height for the model reaction (see Table 5) when the level of calculation rises.

For this small range of temperatures (250−430 K) the experimental values[77] show no curvature in the Arrhenius plot. The present theoretical results in the common temperature range show a very slight curvature of the Arrhenius plot, which was more evident when a larger range of temperatures was analyzed (values not shown). Clearly, this is the expected behavior in a reaction with a heavy-light-heavy mass combination.

The activation energy can be obtained from total rate constants through the usual definition

$$E_a = -R\, d(\ln k)/d(1/T) \tag{4}$$

which is equivalent to determining the slope of the Arrhenius plot. The values are 4.31 and 2.63 kcal mol^{-1} for the scaled- and fitted-Level 0 schemes, respectively, versus the experimental value,[77] 3.00±0.24 kcal mol^{-1}.

3.7. Tropospheric Lifetimes. Fluorinated ethers are regarded as candidates to replace CFCs. The main process for their removal from the atmosphere is the reaction with hydroxyl radicals.

To estimate their lifetime in the troposphere, two approximations were used. In the simplest approximation,[78,79] the tropospheric residence time is given by

$$\tau_{\text{ether}} = (k_{\text{ether}}[\text{OH}])^{-1} \tag{5}$$

where [OH] = 1.1×10^6 molecules cm^{-3} (ref 80). With this work's rate constant calculated at 277 K, the calculated lifetime was 6.5 years. With the more sophisticated model of Prather and Spivakovsky,[81] the lifetime is

$$\tau_{\text{ether}} = [k_{\text{MC}}(277)/k_{\text{ether}}(277)]\cdot\tau_{\text{MC}} \tag{6}$$

where $k_{\text{MC}}(277)$ and τ_{MC} are the rate constant at 277 K (6.71×10^{-15} cm^3 molecule^{-1}s^{-1}) and the corrected lifetime (5.7 years) of the methylchloroform (MC) reference, respectively. With this work's rate constant at 277 K (4.91×10^{-15} cm^3 molecule^{-1} s^{-1}), the calculated lifetime was 7.8 years. The agreement between the two estimates (6.5−7.8 years) lends confidence to the models used.

Conclusions

This work has attempted to shed some light on the reaction of OH radicals with the $CF_3CF_2OCH_3$ molecule, which is important in atmospheric chemistry. In a first step, three different OH radical approaches to the fluorinated ether were investigated by using integrated methods: one, when the OH attacks the H

located in the plane of the carbons (approach 1), and the other two (which are symmetric) when the OH attacks an H located out of that plane (approach 2). In each approach, three stationary points were found using the integrated IMOMO method. The first is a hydrogen-bonded complex (CR1 and CR2 for approaches 1 and 2, respectively) which appears at energies lower than the reactants, −2.59 and −1.26 kcal mol^{-1}, respectively, at 298 K and at the highest level used, Level II. The second is properly characterized as a saddle point (SP1 and SP2), with energy 4.44 and 4.52 kcal mol^{-1}, respectively, above the reactants, and under the same conditions. Finally, a third stationary point (CP) was found close to the products, stabilized by three hydrogen bonds, and common to the two approaches. It was characterized as a hydrogen-bond complex and appears at an energy lower than the products, −5.00 kcal mol^{-1}, under the same conditions.

In a second step, the kinetics of the reaction was analyzed using the variational transition-state theory. Fortunately, the similarity between the geometries, frequencies, and energy changes of the stationary points allows one to assume that the dynamics in the two approaches (1 and 2) would be very similar. Thus, the intrinsic reaction path was constructed for approach 1, and the rate constant was calculated for the whole reaction as thrice the rate constant for approach 1. The IMOMO method with CH_4 + OH as the model reaction was used. This method reproduced the shape of the MEP, V_a^G, and ZPE curves given by the model reaction at the highest level, showing that the success of the integrated method is mainly due to the higher-level model system description, the effect of the remaining lower-level fragments being smaller. The variation of the ZPE presented noticeable changes along the reaction path, with a wide minimum in the saddle point zone which causes fairly marked variational effects.

The rate constants were calculated using variational transition-state theory with multidimensional tunneling of small curvature, where the reaction-path was scaled to higher levels of calculation using the single-point calculation technique. Even at high levels, the present theoretical results strongly underestimate the experimental values. This difference can be due to several factors: from kinetic factors (as the only consideration of the small curvature tunneling effect or the treatment of the lowest frequencies as harmonic vibrational modes instead of free rotors), to electronic molecular structure limitations (as the use of incomplete basis sets and the only partial introduction of correlation energy). Note that this latter factor is a general problem in computational chemistry and is not directly related to the integrated method used.

To sum up, the integrated methods show their effectiveness in the description of potential energy surfaces at a very low computational cost, which is especially interesting for the study of large molecules.

Acknowledgment. I am grateful to Prof. Donald G. Truhlar for providing a copy of the GAUSSRATE program, to Dr. José C. Corchado for computational support, and to the Consejeria de Educación, Ciencia y Tecnología, Junta de Extremadura (Spain) (Project No. 2PR01A002) for partial financial support of this work.

References and Notes

(1) Parr, R. G.; Yang, W. *Density Functional Theory of Atoms and Molecules*; Oxford University Press: New York, 1989.
(2) Dreizler, R. M.; Gross, E. K. U. *Density Functional Theory*; Springer-Verlag: Berlin, 1990.
(3) *Density Functional Methods in Chemistry*; Labanowski, J. K., Andzelm, J. E., Eds.; Springer-Verlag: Berlin, 1991.
(4) Bartolotti, L. J.; Flurchick, K. In *Reviews in Computational Chemistry*; Lipkowitz, K. B., Boyd, D. B., Eds.; VCH: Weinheim, 1996; Vol. 7, p 187.
(5) St. Amant, A. In *Reviews in Computational Chemistry*; Lipkowitz, K. B., Boyd, D. B., Eds.; VCH: Weinheim, 1996; Vol. 7, p 217.
(6) Ziegler, T. *Chem. Rev.* **1991**, *91*, 651.
(7) Bauschlicher, C. W. *Chem. Phys. Lett.* **1995**, *246*, 40.
(8) Redfern, P. C.; Zapol, P.; Curtiss, L. A.; Raghavachari, K. *J. Chem. Phys.* **2000**, *104*, 5850.
(9) Johnson, B. G.; González, C.; Gill, P. M. W.; Pople, J. A. *Chem. Phys. Lett.* **1994**, *221*, 100.
(10) Pederson, M. R. *Chem. Phys. Lett.* **1994**, *230*, 54.
(11) Porezag, D.; Pederson, M. R. *J. Chem. Phys*. **1995**, *102*, 9345.
(12) Durant, J. L. *Chem. Phys. Lett.* **1996**, *256*, 595.
(13) Jursic, B. S. *Chem. Phys. Lett.* **1997**, *264*, 113.
(14) Skokov, S.; Wheeler, R. A. *Chem. Phys. Lett.* **1997**, *271*, 251.
(15) Tozer, D. J.; Handy, N. C. *J. Phys. Chem.* **1998**, 102, 3162.
(16) Proynov, E.; Chermette, H.; Salahub, D. R. *J. Chem. Phys*. **2000**, *113*, 10021.
(17) Lynch, B. J.; Truhlar, D. G. *J. Phys. Chem*. **2001**, *105*, 2936.
(18) Lynch, B. J.; Fast, P. L.; Harris, M.; Truhlar, D. G. *J. Phys. Chem. A* **2000**, *104*, 21.
(19) Poater, J.; Solá, M.; Durán, M.; Robles, J. *Phys. Chem. Chem. Phys.* **2002**, *4*, 722.
(20) Warshel, A.; Levitt, M. *J. Mol. Biol.* **1976**, *103*, 227.
(21) Singh, U. C.; Kollman, P. A. *J. Comput. Chem.* **1986**, *7*, 718.
(22) Field, M. J.; Bash, P. A.; Karplus, M. *J. Comput. Chem.* **1990**, *11*, 700.
(23) Eckert, J.; Kubas, G. J.; Hall, J. H.; Hay, P. J.; Boyle, C. M. *J. Am. Chem. Soc.* **1990**, *112*, 2324.
(24) Warshel, A. *Computer Modeling of Chemical Reactions in Enzymes and Solutions*; John Wiley & Sons: New York, 1991.
(25) Kawamura, H.; Koga, N.; Morokuma, K. *J. Am. Chem. Soc*. **1992**, *114*, 8687.
(26) Maseras, F.; Koga, N.; Morokuma, K. *Organometallics* **1994**, *13*, 4008.
(27) Maseras, F.; Morokuma, K. *J. Comput. Chem.* **1995**, *16*, 1170.
(28) Humbel, S.; Sieber, S.; Morokuma, K. *J. Chem. Phys.* **1996**, *105*, 1959.
(29) Svensson, M.; Humbel, S.; Morokuma, K. *J. Chem. Phys.* **1996**, *105*, 3654.
(30) Svensson, M.; Humbel, S.; Froese, R. D. J.; Matsubara, T.; Sieber, S.; Morokuma, K. *J. Phys. Chem.* **1996**, *100*, 19357.
(31) Coitiño, E. L.; Truhlar, D. G.; Morokuma, K. *Chem. Phys. Lett.* **1996**, *259*, 159.
(32) Coitiño, E. L.; Truhlar, D. G. *J. Phys. Chem*. **1997**, *101*, 4641.
(33) Noland, M.; Coitiño, E. L.; Truhlar, D. G. *J. Phys. Chem.* **1997**, *101*, 1193.
(34) Gao, J. *Rev. Comput. Chem.* **1996**, *7*, 119.
(35) Corchado, J. C.; Truhlar, D. G. *J. Phys. Chem.* **1998**, *102*, 1895.
(36) Corchado, J. C.; Truhlar, D. G. In *Combined Quantum Mechanical and Molecular Mechanical Methods*, ACS Symposium Series, Vol. 712; Gao, J., Thompson, M. A., Eds.; (ACS, Washington, D. C.) pag. 106, **1998**.
(37) Dapprich, S.; Komaromi, I.; Byun, K. S.; Morokuma, K.; Frisch, M. J. *J. Mol. Struct.* (*Theochem*) **1999**, *461*, 1.
(38) Espinosa-García, J. *Phys. Chem. Chem. Phys*. **2002**, *4*, 1807.
(39) Zhang, Y.; Liu, H.; Yang, W. *J. Chem. Phys.* **2000**, *112*, 3483.
(40) Truong, T. N.; Duncan, W. T.; Tirtowidjojo, A. *Phys. Chem. Chem. Phys.* **1999**, *1*, 1061.
(41) Truong, T. N.; Truong, T.-T. *Chem. Phys. Lett.* **1999**, *314*, 529.
(42) Truong, T. N.; Maity, D. K.; Truong, T.-T. *J. Chem. Phys.* **2000**, *112*, 24.
(43) Espinosa-García, J.; Corchado, J. C. *J. Chem. Phys.* **2001**, *115*, 3021.
(44) Espinosa-García, J. *J. Phys. Chem. A* **2002**, *106*, 5686.
(45) Doubleday, C.; McIver, J. W.; Page, M. *J. Phys. Chem.* **1988**, *92*, 4367.
(46) Baldridge, K. M.; Gordon, M. S.; Steckler, R.; Truhlar, D. G. *J. Phys. Chem.* **1989**, *93*, 5107.
(47) Truhlar, D. G.; Gordon, M. S. *Science* **1990**, *249*, 491.
(48) Truhlar, D. G.; Isaacson, A. D.; Garrett, B. C. In *The Theory of Chemical Reactions*; Baer, M., Ed.; CRC: Boca Raton, FL, 1985; Vol. 4.
(49) Bondi, D. K.; Connor, J. N. L.; Garrett, B. C.; Truhlar, D. G. *J. Chem. Phys.* **1983**, *78*, 5981.
(50) Frisch, M. J.; Trucks, G. W.; Schlegel, H. B.; Scuseria, E.; Robb, M. A.; Cheeseman, J. R.; Zakrzewski, V. G.; Montgomery, J. A.; Stratman, R. E.; Burant, J. C.; Dapprich, S.; Millam, J. M.; Daniels, A. D.; Kudin, K. N.; Strain, M. C.; Farkas, O.; Tomasi, J.; Barone, V.; Cossi, M.; Cammi, R.; Menucci, B.; Pomelli, C.; Adamo, C.; Clifford, S.; Ochterki, J.; Petterson, G. A.; Ayala, P. Y.; Cui, Q.; Morokuma, K.; Malik, D. K.; Rabuk, A. D.; Raghavachari, K.; Foresman, J. B.; Cioslowski, J.; Ortiz, J. V.; Stefanov, J. J.; Liu, G.; Liashenko, A.; Piskorz, P.; Komaromi, I.; Gomperts, R.; Martin, R. L.; Fox, D. J.; Keith, T.; Al-Laham, M. A.; Peng, C. Y.; Nanayakkara, A.; González, C.; Challacombe, M.; Gill, P. M. W.; Johnson,

B. G.; Chen, W.; Wong, M. W.; Andres, J. L.; Head-Gordon, M.; Reploge, E. S.; Pople, J. A.; GAUSSIAN98 program, Revision A.7, Gaussian Inc.: Pittsburgh, PA 1998.

(51) Bartlett, R. J. *J. Phys. Chem*. **1989**, *93*, 1697.

(52) Kendall, R. A.; Dunning, T. H.; Harrison, R. J. *J. Chem. Phys*. **1992**, *96*, 6796.

(53) Isaacson, A. D.; Truhlar, D. G. *J. Chem. Phys*. **1982**, *76*, 1380.

(54) Miller, W. H.; Handy, N. C.; Adams, J. E. *J. Chem. Phys*. **1980**, *72*, 99.

(55) Garrett, B. C.; Truhlar, D. G. *J. Am. Chem. Soc*. **1979**, *101*, 4534.

(56) Corchado, J. C.; Coitiño, E. L.; Chuang, Y.-Y.; Truhlar, D. G. GAUSSRATE, Version 8.0/P8.0-G94; University of Minnesota: Minneapolis, MN, 1998.

(57) Chuang, Y. Y.; Corchado, J. C.; Fast, P. L.; Villá, J.; Coitiño, E. L.; Hu, W. P.; Liu, Y. P.; Lynch, G. C.; Nguyen, K.; Jackells, C. F.; Gu, M. Z.; Rossi, I.; Clayton, S.; Melissas, V.; Steckler, R.; Garrett, B. C.; Isaacson, A. D.; Truhlar, D. G. POLYRATE Version 8.4, University of Minnesota: Minneapolis, 1999.

(58) Truhlar, D. G. *J. Comput. Chem.* **1991**, *12*, 266.

(59) Jackels, C. F.; Gu, Z.; Truhlar, D. G. *J. Chem. Phys*. **1995**, *102*, 3188.

(60) Chuang, Y. Y.; Truhlar, D. G. *J. Phys. Chem.* **1997**, *101*, 3808.

(61) Natanson, G. A.; Garrett, B. C.; Truong, T. N.; Joseph, T.; Truhlar, D. G. *J. Chem. Phys*. **1991**, 94, 7875.

(62) Espinosa-García, J.; Corchado, J. C. *J. Phys. Chem.* **1996**, *100*, 16561.

(63) Lu, D. H.; Truong, T. N.; Melissas, V. S.; Lynch, G. C.; Liu, Y. P.; Garrett, B. C.; Steckler, R.; Isaacson, A. D.; Rai, S. N.; Hancock, G. C.; Lauderdale, G. C.; Joseph, T.; Truhlar, D. G. *Comput. Phys. Commun*. **1992**, *71*, 235.

(64) Truong, T. N.; Lu, D.-H.; Lynch, G. C.; Liu, Y. P.; Melissas, V. S.; Stewart, J. J.; Steckler, R.; Garrett, B. C.; Isaacson, A. D.; González-Lafont, A.; Rai, S. N.; Hancock, G. C.; Joseph, T.; Truhlar, D. G. *Comput. Phys. Commun*. **1993**, *75*, 43.

(65) Hammond, G. S. *J. Am. Chem. Soc*. **1955**, *77*, 334.

(66) Malik, D. K.; Petersson, G. A.; Montgomery, J. A. *J. Chem. Phys.* **1998**, *108*, 5704.

(67) Aliagas, I.; Gronert, S. *J. Phys. Chem.* **1998**, *102*, 2609.

(68) Korchowiec, J.; Kawakara, S. I.; Matsumura, K.; Uchimaru, T.; Surgie, M. *J. Phys. Chem. A* **1999**, *103*, 3548.

(69) Masgrau, L.; González-Lafont, A.; Lluch, J. M. *J. Chem. Phys.* **2001**, *114*, 2154.

(70) Lynch, B. J.; Truhlar, D. G. *J. Chem. Phys.* **2002**, *106*, 842.

(71) Espinosa-García, J.; Corchado, J. C. *J. Chem. Phys.* **1994**, *101*, 8700.

(72) Espinosa-García, J.; Coitiño, E. L.; González-Lafont, A.; Lluch, J. M. *J. Phys. Chem.* **1998**, *102*, 10715.

(73) Espinosa-García, J.; Corchado, J. C. *J. Chem. Phys.* **1994**, *101*, 1333.

(74) Espinosa-García, J. *J. Phys. Chem. A* **2000**, *104*, 7537.

(75) Melissas, V. S.; Truhlar, D. G. *J. Chem. Phys.* **1993**, *99*, 1013.

(76) Espinosa-García, J.; Corchado, J. C. *J. Chem. Phys.* **2000**, *112*, 5731.

(77) Tokuhashi, K.; Takahashi, A.; Kaise, M.; Kondo, S.; Sekiya, A.; Yamashita, S.; Ito, H. *Int. J. Chem. Kinet.* **1999**, *31*, 846.

(78) Francisco, J. S. *J. Chem. Phys.* **1992**, *96*, 7597.

(79) Atkinson, R. *Chem. Rev.* **1985**, *85*, 192.

(80) Miller, B. R.; Huang, J.; Weiss, R. F., Prinn, R. G.; Fraser, P. J. *J. Geophys. Rev.* **1998**, *103*, 13237.

(81) Prather, M.; Spivakovsky, C. M. *Geophys. Res.* **1990**, *95*, 723.